http://dx.doi.org/10.7735/ksmte.2016.25.6.410

J. Korean Soc. Manuf. Technol. Eng.
ISSN 2508-5107(Online) / ISSN 2508-5093(Print)

Controlling the Depth of Microchannels Formed during Rolling-based Surface Texturing

Quang-Thanh Bui[a,b], Seung-Kook Ro[a,b*], Jong-Kweon Park[a,b]

[a] *Department of Nano-Mechatronics, Korea University of Science and Technology, 217, Gajeong-ro, Yuseong-gu, Daejeon 34113, Korea*
[b] *Department of Ultra-Precision Machine and System, Korea Institute of Machinery and Materials, 156, Gajeongbuk-ro, Yuseong-gu, Daejeon 34103, Korea*

ARTICLE INFO

Article history:
Received 2 November 2016
Revised 12 December 2016
Accepted 14 December 2016

Keywords:
Micro-rolling
Position control
Surface texturing
Micro-forming
Compliant mechanism

ABSTRACT

The geometric dimension and shape of microchannels that are formed during surface texturing are widely studied for applications in flow control, and drag and friction reduction. In this research, a new method for controlling the deformation of U channels during micro-rolling-based surface texturing was developed. Since the width of the U channels is almost constant, controlling the depth is essential. A calibration procedure of initial rolling gap, and proportional-integral PI controllers and a linear interpolation have been applied simultaneously to control the depth. The PI controllers drive the position of the pre-U grooved roll as well as the rolling gap. The relationship between the channel depth and rolling gap is linearized to create a feedback signal in the depth control system. The depth of micro channels is studied on A2021 aluminum lamina surfaces. Overall, the experimental results demonstrated the feasibility of the method for controlling the depth of microchannels.

1. Introduction

Micro surface texturing has emerged as a non-conventional technology to reduce drag, friction and wear or control the flow in fluid dynamics. It is applicable in various fields such as hydrodynamic bearing lubrication, modern aviation and high-speed rail industries, artificial body parts in medical field, etc. There have been many research reports that tribology and fluid flow characteristics in textured surface are sensitive to dimensional parameters, density and shape of the micro-channels or dimples[1-3]. Fredrik et al.[4] investigated the influences of groove depth and width, Reynolds number and geometrical shape on surface texturing to the flow, load carrying capacity and friction force in hydrodynamic lubrication of two parallel surfaces. Aviram et al.[5] presented a numerical study where Reynolds equation is used to demonstrate the effects of spherical micro-pores applied on a stationary surface in hydrodynamic lubrication. A change of the area density of pores in the range between 5% and 20% varies the friction force by less than 7% and an optimal value of the pore depth over diameter ratio was found, which yields a minimum friction force. Shinkarenko et al.[6] developed a theoretical model to optimize a dimple density and an aspect ratio including dimple depth and radius for maximum carrying load and minimum friction on rod seals and piston rings. With the same purpose, Christos et al.[7] also studied on genetic algorithms to optimize trapezoidal channels on thrust bearings.

For the essential needs of fabricating micro channels and

* Corresponding author. Tel.: +82-42-868-7115
Fax: +82-42-868-7180
E-mail address: cniz@kimm.re.kr (Seung-Kook Ro).

dimples, many texturing methods such as laser ablation, photochemical etching are researched and developed on flat, spherical and cylindrical surfaces[8,9]. In regard to the field of micro surface texturing on large-area of metal lamina with an economical and environmental-friendly way, a novel rolling-based surface texturing system is developed to make various shapes and control over the geometrical dimension of micro channels. Figure 1(a) shows a concept of deformation-based micro surface texturing. The operating principle, design and analysis details of a fully developed micro-rolling system are described in sections 2.1 and 2.2. Differing tooth shapes can be used on the upper pre-textured roll, such as U-groove, V-groove, and semi-circular C-groove, to enable the creation of diverse shapes and densities on the lamina surface by single patterning or grid patterning[10]. Figure 1(b) presents two micro surface texturing processes, the single patterning makes micro channels and the grid patterning makes grid-pattern on lamina surface.

Among crucial factors affecting to the tribology and fluid flow behavior of the textured surfaces, the dimensional parameters such as the width and depth of micro-channels are controllable in texturing process. In this paper, an upper pre-U grooved roll was employed to imprint rectangular channels on a lamina surface in experiments. Since the width of the channels is almost constant, the main goal is to control over the depth of rectangular micro-channels precisely. According to geometrical relation in Fig. 1, controlling the rolling gap and the parallelism of two rollers are two difficult problems dominating the depth and width of micro-channels. To solve these, the PI control method described in section 2.3 is to position the upper roller under rolling forces F_0 and F_1 to push down toward smaller rolling gaps for forming the channels. A calibration procedure of the rolling gap is described in section 3.2 to set up the initial gap and the parallelism. In sections 3.3 and 3.4, a novel method is proposed to coordinately use PI controllers and a linear interpolation method to control over the depth. The linear interpolation method is to find out a relationship between the channel depth and the gap for creating a feedback signal in building the control over the depth system. Detailed discussions and conclusions of the results are reported in section 4.

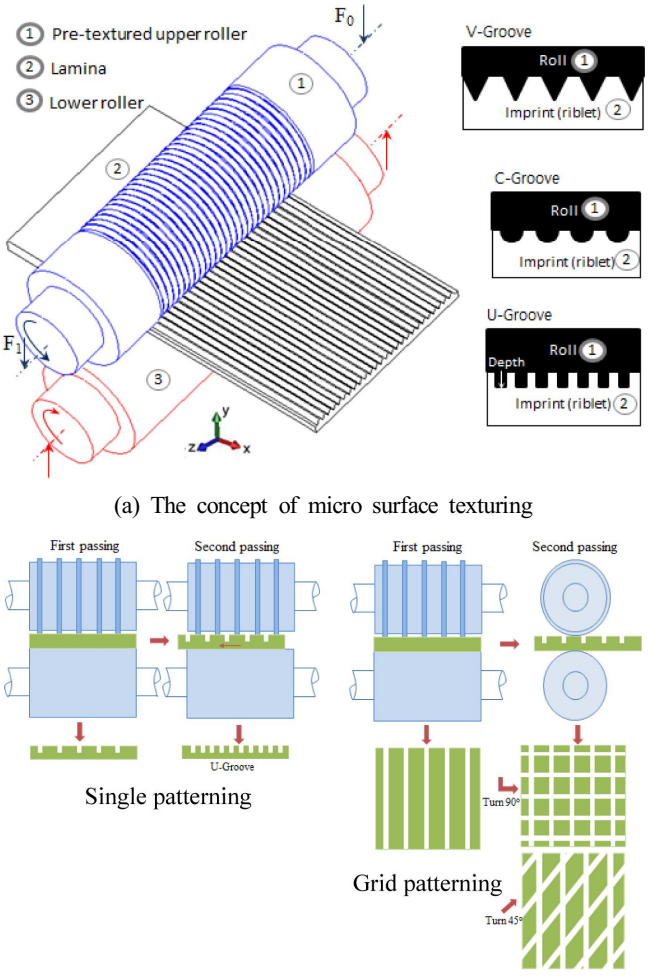

(a) The concept of micro surface texturing

(b) Micro surface texturing process

Fig. 1 Illustration of the concept of deformation-based micro surface texturing

2. Desktop Micro-rolling System

2.1 Introduction to the Micro-rolling System

A desktop micro-rolling machine (*DμRM*) was designed to realize the concept of micro-rolling-based surface texturing, and control over the depth of the micro-channels on metal lamina needs handling in this research. Adjusting rolling forces F_0 and F_1 requires at least a movable roller, as shown in Figure 1. Figure 2 shows a schematic diagram of the *DμRM*. The upper and lower rollers were attached on shafts, which were powered using two direct-current (DC) motors, where the speed was controlled using inverters. The machine structure can be described in terms of the upper and lower parts. The upper part consists of an upper roll, a positioning unit that includes two screw tips, piezoelectric actuators (PZT), piezoelectric load cells (Kistler 9001A), ball tips and guide blocks at both sides of the upper roller. By adjusting the screw tips, the backlash along the actuators to the guide blocks may be eliminated. The ball tips were attached to the head of the actuators, and were used to prevent damage to the actuators due to tilting and shearing forces. The actuators were

electromechanical transducers, and provide extremely small displacements (in the sub-nanometer range) with a large stiffness and a fast response[11]. However, the actuators were formed of a dielectric material that suffered from nonlinear and hysteretic behavior. This characteristic electrical behavior affects to the micro adjustment and control. There are several models of hysteresis, and associated control methods to compensate for the hysteretic behavior of the actuators[12]. The stroke of the actuators provides flexure guide block displacement, and a load cell was used to monitor the rolling force. The guide block was designed to enable vertical motion over a wide range with nanometer resolution, a high stiffness and a large bandwidth.

The lower part consisted of a lower roller, flexure guide blocks, and a wedge unit. The position of the lower roller could be adjusted by repositioning the wedge unit. The separation between the two rolls was accurately detected via the two position sensors (MicroSense 2810). A controller was connected via amplifiers and an I/O unit, was used to manage the operation of the actuators, load cells and position sensors. In this research, a smooth fixed lower roller was used with a pre-U-grooved upper roller to imprint rectangular channels on a lamina surface. The width, density and shape of the rectangular micro-channels were almost constant. Therefore, the depth of the micro-channels affects the efficiency of the flow, drag and friction in the lubricant environment critically. Research aim is to control the depth of the micro-channels. The depth of micro channels is determined by the rolling forces F_0 and F_1, which create pressure to imprint the tooth shape of the upper roll on the top surface. Whereas the lower roller is fixed, the forces F_0 and F_1 will depend on the position of the upper roller. Hence, control over the depth of channels can be achieved by varying the position of the upper roller.

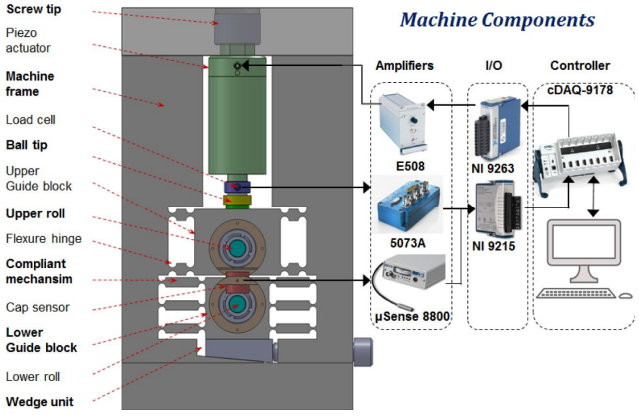

Fig. 2 Schematic diagram of the desktop micro-rolling machine

2.2 Analysis and Measurement of Flexure Guide Block'S Stiffness

Piezoelectric-driven compliant mechanisms are widely used in micro/nano positioning systems, and were employed here to position the upper roller in the *DμRM*. Evaluations of the safety factor and working ability of the upper roller need to be solved. Figure 3 shows a 3D rendering and dimensional parameters of the upper guide block, a compliant mechanism, which was comprised of a bearing housing linked to the main frame via a compliant mechanism to provide elastic deformation. The compliant mechanism includes two circular flexure hinges with low rotational stiffness in one axis and high stiffness in the other degree of freedom (DOF).

The flexure hinges were connected via a linkage to magnify the range of motion. The guide block could be translated vertically while constraining the other DOF. The flexure guide block has no friction, clearance and lubrication so can eliminate certain errors in order to achieve a high resolution. Stiffness of the flexure guide block need to be determined to constituting a measurement and control system for the position of upper roller. To control the position of the upper roll, the range of motion and safety factor of the guide block should also be known. Figure 4 shows a force and deformation analysis of the guide block. With an applied force F, linkage length L and flexure circular hinges with an angle of rotation θ, the guide block will undergo a displacement y. These parameters depend on requirements for the stiffness and movable range of the guide block[13-16].

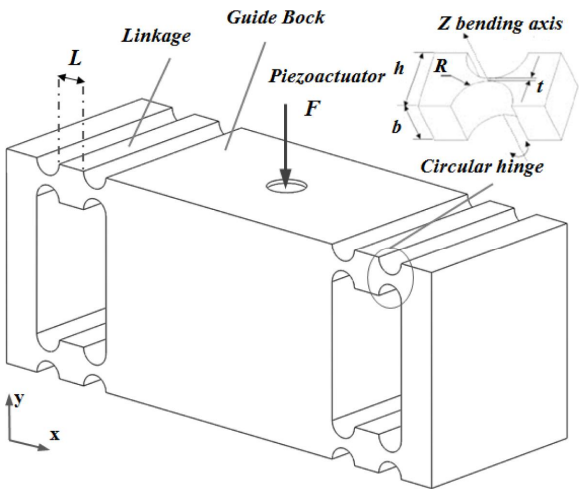

Fig. 3 3D rendering of the upper guide block

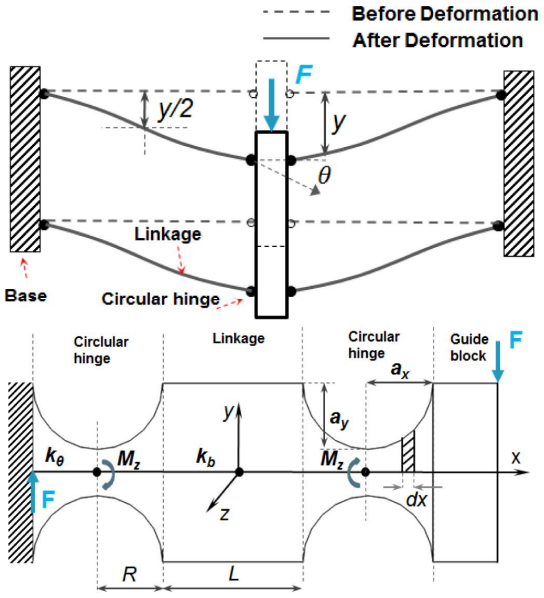

Fig. 4 Force and deformation analysis on the upper guide block

An analytical calculation is proposed to solve the stiffness and design parameters of flexure guide block. Based on bending theory, the angular stiffness of the circular flexure hinge is as follows:

$$\theta = \int_{-R}^{R} \frac{M_z}{EI_z} dx = \int_{-R}^{R} \frac{12M_z}{Eb(2yx)^3} dx = \frac{3M_z a_x}{2Eba_y^3} \int_{-\pi/2}^{\pi/2} \frac{\cos\theta}{((1+t/2a_y)-\cos\theta)^3} d\theta \quad (1)$$

where $x = \alpha\sin\theta$, the elastic modulus E=200 Gpa, an approximate solution for the angular compliance was first presented by Paros and Weisbord in 1965[17], and the angular stiffness K_θ is given by:

$$K_\theta = \frac{M_z}{\theta} = \frac{2Ebt^{5/2}}{9\pi R^{1/2}} \quad (2)$$

The compliant mechanism includes two circular flexure hinges and a linkage can be described by considering conservation of energy; i.e.,

$$\frac{1}{2}F\frac{y}{2} = \frac{1}{2}K_\theta\theta^2 + \frac{1}{2}K_b(\frac{y_b}{2})^2 \quad (3)$$

The beam was very stiff, the vertical displacement of the single beam can be approximated to $y_b \sim 0$ and relationship between angle of rotation θ and displacement of the guide block y is given by:

$$y = \theta(2R+L) \quad (4)$$

The relationship between force and deformation of a compliant mechanism is described from Eqs. (3) and (4) as:

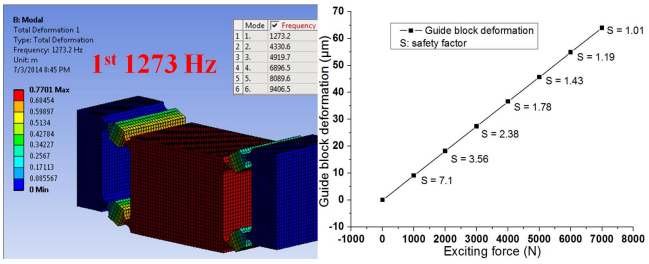

(a) (b)

Fig. 5 (a) FEM modal analysis of the flexure guide bock and (b) the corresponding structural analysis

$$F = K_\theta \frac{2y}{(2R+L)^2} \quad (5)$$

There are four compliant mechanisms attached to the upper guide block, so the stiffness of the upper guide block is given by:

$$K_s = 4\frac{F}{y} = \frac{8}{(2R+L)^2}K_\theta \quad (6)$$

The maximum displacement of the mechanism ymax corresponding to the maximum bending torque, given as:

$$y_{max} = \theta_{max}(2R+L) = M_{zmax}(2R+L)/K_\theta = \frac{\sigma_{yield} I_{zmin}}{K_\theta t/2}(2R+L) = \frac{\sigma_{yield} bt^2}{6K_\theta}(2R+L) \quad (7)$$

where I_{zmin} is the minimum moment of inertia of the hinge about the bending axis z. The yield strength of structural steel σ_{yield} =250 MPa. Eqs. (2)~(7) are fundamentals of the guide block design. Dimensional parameters of the guide block are primarily calculated from design specifications such as stiffness K_s, movable range y_{max} and maximum exciting force F_{max}. The finite element method (FEM) can be used as part of a modal and structural analysis to investigate the resonant frequencies, deformation and safety factor of the guide block in the vertical direction y. This represents another method of determining K_s, and furthermore, to investigate the safety factor S of the guide block structure according to von-Mises yield criterion. Figure 5(a) shows the results of a modal analysis, whereby the maximum deformation was δ_{max}=0.77 m, which occurred with a resonant frequency f=1,273.2 Hz. The effective modal mass and the stiffness of the guide block are given by

$$m_{eff} = 1/\delta_{max} \quad (8)$$

$$K_s = w^2 m_{eff} \quad (9)$$

where $w=2\pi f$. So the stiffness was K_s=1.08×10^8 N/m and the

compliance was C_s=1/K_s=9.2×10^{-9} m/N. Figure 5(b) shows structural analysis results, which reveals the strength limitation of the guide block structure with an applied force of F =7,000 N, the allowable stroke is 64 μm, safety factor S=1.01.

An open-loop system was used to measure the displacement of the guide block in response to an applied force, where the stiffness of the flexure block can be estimated experimentally. The open-loop system can also measure the inherent hysteresis in the actuator, as well as enable a manual mode of adjusting the position of guide block.

Figure 6 shows a schematic diagram of the open-loop measurement system. The actuator model was a P-235.80, and amplifier model was an E-508.00, both from Physik Instruments, and the amplifier gain was K_a=100. When a voltage is applied across the actuator, the length of the actuator changes so as to translate the guide block through the load cell to monitor the force F. K_f is the ratio of the applied voltage to the output force, and was determined experimentally. The applied voltage was in the range 0~9 V, which was constrained to avoid damage to the actuator. Figure 6(a) shows the inherent hysteresis of the actuator and displacement of the guide block y in the range 0~44 μm. Simultaneously, the exciting force F is measured in the range 0~4900 N. So K_a×K_f=4900/9, which implies that K_f=4900/(9×100)=5.44. Figure 6(b) shows the relationship between the vertical displacement of guide block y and the force F. The static

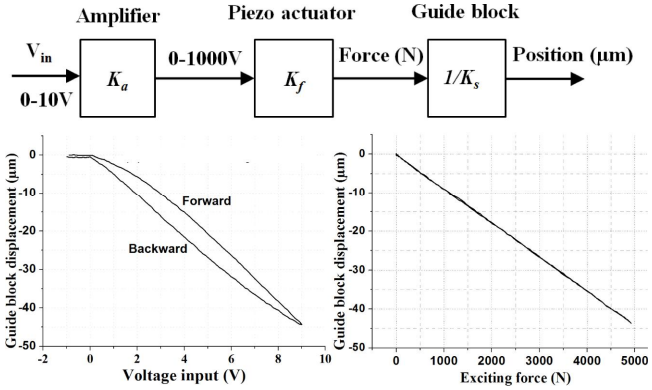

(a) PZT inherent hysteresis (b) Force-displacement curve

Fig. 6 A schematic diagram of the open-loop measurement system and the experimental results

Table 1 Dimensional parameters and stiffness results of the upper guide block

	b (m)	h (m)	R (m)	Results	K_s (N/μm)
8e-3	5e-2	1e-2	3.7e-3	Experiment	111
				FEM	108

stiffness of the guide block was K_s=F/y=111 N/μm, and the compliance was C_s=1/K_s=44/4900=0.009 μm/N.

A comparison between FEM analysis and measurement results reveals a good agreement. Finally, design parameters, measurement and analysis results of upper guide block are listed in Table 1. The experimental data is used in the following sections.

2.3 Control System for Positioning the Upper Roll

The open-loop system was designed to evaluate and adjust the primary parameters of the desktop micro rolling machine. A closed-loop control system, however, is required to control the actuator. The separation between the rollers is one of the major factors affecting the channel size. Because the lower roll is fixed, control over the position of the upper roller will determine this gap. Furthermore, the gap must be stable across texturing process. To meet these demands, compensation for the inherent hysteresis is required, and a closed-loop control system for the position of the upper roller was implemented. This method can improve the rolling accuracy and the quality of the resulting surface texture, and enables rapid set-up of the machine. The upper roll was attached via a shaft located on two guide blocks, and so positioning guide blocks are used to control the position of the upper roll. Proportional-integral-derivative (PID) controllers are widely used for applications that require accurate positioning; however, a proportional-integral (PI) controller is more attractive in the practice because the gain at higher frequencies remains finite[18-22].

In Figure 7, the controller improves the transient response and steady-state error e. Transfer functions for each subsystem are defined as the following:

$$\frac{y_c}{e} = K_p + \frac{K_i}{s} \tag{10}$$

$$\frac{V_{in}}{y_c}(s) = T \tag{11}$$

$G(s)$ is second-order transfer function of the Piezo-driven compliant mechanism. T=1,000 V/120 μm is the ratio converting voltage to displacement. y_e, y are the input and output

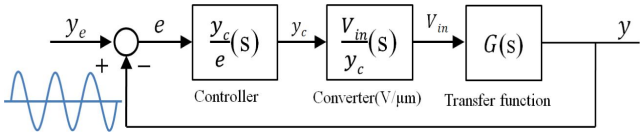

Fig. 7 The PI control model for positioning the guide block

values of the guide block position, $e=y_e-y$ is error in positioning. The term K_p is the proportional gain constant, and significantly affects the output. An excessively large K_p can result in an unstable loop; however, an excessively small K_p results in a small output response to a large input; i.e., a less sensitive controller. K_i is the integral gain, and accelerates the motion toward the reference point and eliminates the residual steady-state error. However, since K_i responds to accumulated errors from previous input controls, it can result in overshoot.

The actuators used for guide block positioning provide motion in the vertical direction. With the *DμRM*, the upper roll was installed on the shaft attached on two guide blocks, and so has 2 DOFs. Figure 8 shows a schematic diagram of the positioning control system of the upper roller.

Two PI controllers were used to control the actuators. The position and the angle of the upper roll relative to the horizontal (i.e., *x*-axis) is given by

$$y = (y_0 + y_1)/2 \quad (12)$$

$$\varphi = |y_0 - y_1|/l \quad (13)$$

where y_0 is the position of the left guide block, y_1 is the position of the right guide block, and l is the length of the shaft. The PI control system was built with a cDAQ-9178, an NI-9215 and an NI-9263 using Labview. The PI gains were tuned from small to large to determine appropriate values. The control system operated stably with a proportional gain of K_p =0.04 and an integral gain of K_i=0.00001 for both sides.

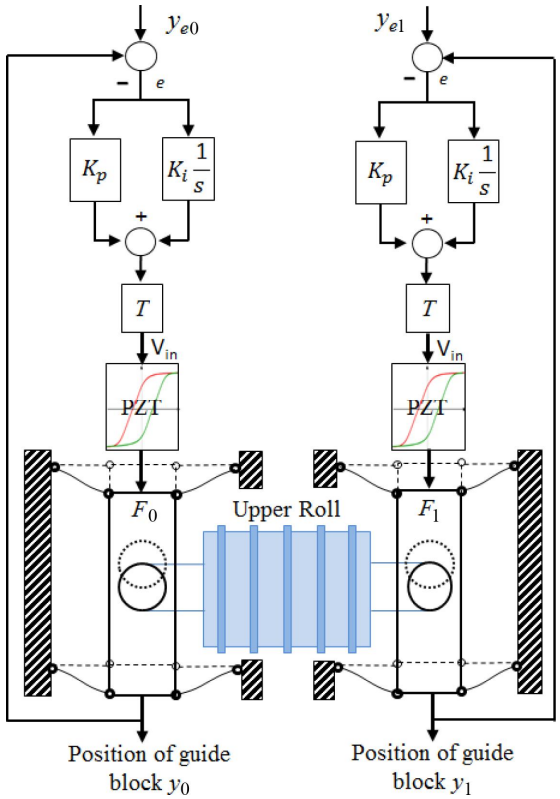

Fig. 8 Scheme of control system for positioning the 2-DOF upper roller

An experiment was carried out to investigate the control over the upper roller with a reference position of y_e=15 μm; i.e., the reference position of the left guide block was y_{e0}=15 μm and the reference position of right guide block was y_{e1}=15 μm. Figure 9(a) shows the position of the guide blocks and Figure 9(b) shows the error. The roll was translated toward y=15 μm with a response time of t=1.6 s. The error is shown in Figure 9(c); the maximum error was e=0.13 μm. Figure 9(d) shows the angular error; the maximum angular error was 2.5×10^{-6}. The PI controller for positioning the upper roll is an important aspect of investigating the channels formed with the *DμRM*, as described in the following section.

3. Experiment Setup and Results on Forming and Control Over the Depth of Micro Channels

3.1 Textured Roll

In this research, the lower roller of the DμRM had a smooth surface and was machined from tool steel and heat-treated to

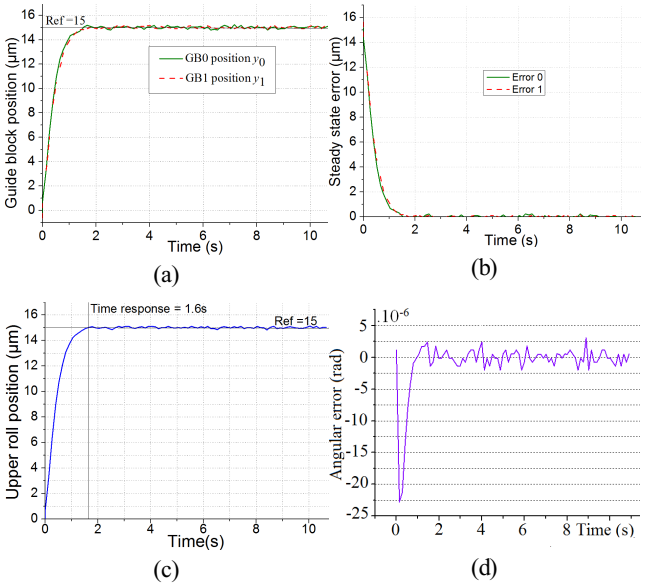

Fig. 9 Experimental results of the positioning of the upper roll (a) The position of the guide blocks (b) the position error (c) the position of upper roll (d) the rotational angle of the roller ϕ

achieve the required hardness. A pre-textured roll was employed to operate with a smooth lower roll to generate rolling pressure for imprinting channels on the top surface of the lamina via a single pass with each experiment.

The pre-textured roll was formed of tungsten carbide and fabricated by grinding to create a U-groove toothed configuration. The tooth width was w_t=60 μm, the tooth height was 110 μm, and the tooth pitch was a=350 μm, as shown in Figure 10.

3.2 Calibration Procedure of the Initial Rolling Gap

The rolling gap will dominate the rolling forces F_0 and F_1 compressing on the lamina surface to make the micro-channels. Calibration of initial gap is the primary step to achieve control over the rolling gap. In Figure 11(a), the parallelism and the initial rolling gap G was determined from the gaps G_0 and G_1 between the upper and lower rolls at either side of rolls. First, the lower roll is coarsely adjusted using the bottom wedge unit. After the lower roll was fixed, the upper adjusting unit with nanometer accuracy was used for fine adjustment in real-time during the surface-texturing process. Two ultra-precision actuators were used to locate the left and right upper guide blocks independently. A thickness gage (see Figure 11(b)) was used to measure the initial gap roughly, and then two noncontact capacitive position sensors and two load cells were used to measure the initial gap with micron resolution. In this way, the initial gap can be calculated and tilt of the rolls can be detected easily.

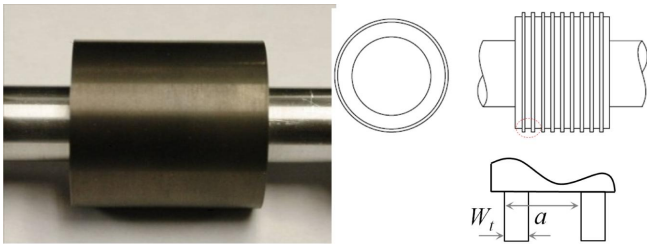

Fig. 10 The configuration of the pre-textured roll

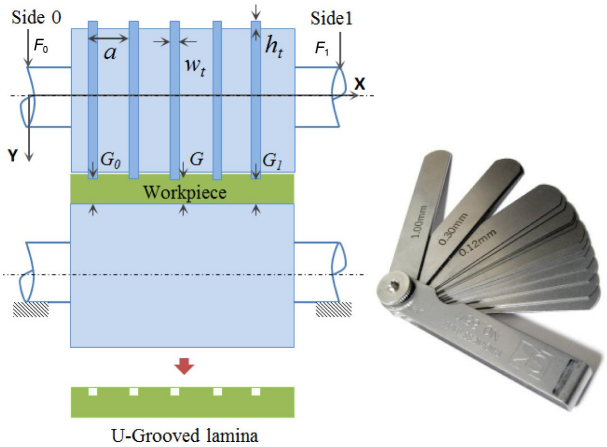

(a) (b)

Fig. 11 (a) configuration of rolling gap and pre-textured roll (b) thickness gage

Figure 12 shows a flowchart of the calibration of the initial gap. The thickness gage had a resolution of 10 μm, and sufficient hardness for use as a thickness gage to calibrate the gap. Zero offsets were set for the capacitive sensors because at the initial positions y_0 and y_1 of guide blocks, non-zero forces F_0 and F_1 may exist after the installation process. During adjustment of the wedge unit at the bottom, a thickness gauge which can be selected in different thicknesses t was placed on the left and right sides of the rolls, respectively, to estimate the gaps G_0, G_1 and monitor the forces F_0, F_1 through using the load cells. The thickness gage could slip through the gap G_0 with t=0.85 mm but got stuck on t=0.86 mm. The thickness gage could get through the gap G_1 with t=0.84 mm, got stuck on t=0.85 mm. Therefore $850<G_0<860$ μm and $840<G_1<850$ μm. Thickness gage was inserted with t=0.85 mm in the gap G_0 and t=0.84 mm in the gap G_1. Subsequently, the guide blocks are pushed down by driving the actuators $y_i(i=0,1)$ from 1 μm to 10 μm in steps of 1 μm and the load cells were simultaneously monitored. F_1' and F_i are values of load cells in cases of attached

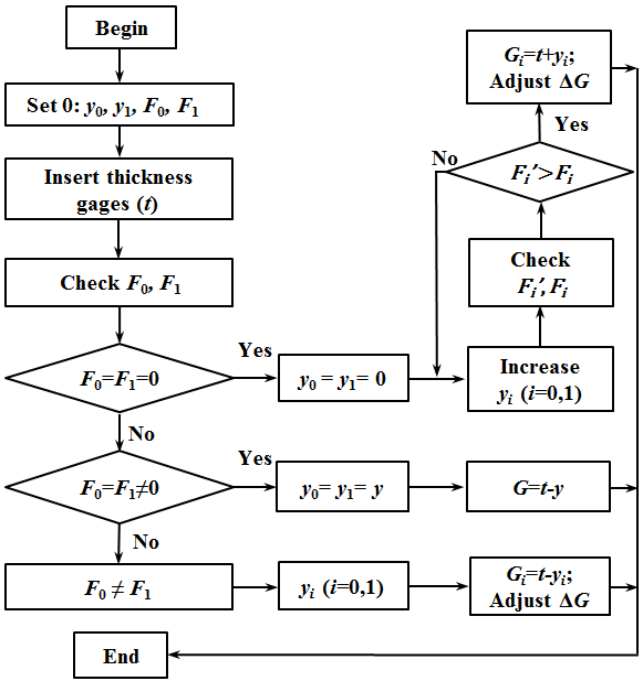

Fig. 12 Flowchart showing the calibration procedure

thickness gage and detached thickness gage, respectively. The gap was then adjusted to remove the tilting error.

The results are $F_0^{'}>F_0$ initially with y_0=8 μm and $F_1^{'}>F_1$ initially with y_1=1 μm, therefore, $G_0=t_0+8$=858 μm and $G_1=t_1+1$=841 μm, respectively. It follows that the tilting error was $\triangle G=|G_0-G_1|$=17 μm, which should be eliminated. Here, G_0 decreased by 8 μm and G_1 increased by 9 μm to set the initial rolling gap at $G=G_0=G_1$=850 μm.

3.3 Relationship between the Depth of the Micro-channels and the Position of the Upper Roller

To determine the relationship between the depth of the micro-channels and position of the upper roller, experiments are implemented on aluminum A2021 lamina 40×20×1 (mm) with the initial rolling gap at G=850 μm. The channel depth was investigated using an empirical method with designated position of the upper roll displacement y_e=0, 10, 20, 28 and 34 (μm). With each position, the depth of the channels was inspected 3 times and the mean was calculated. Linear interpolation in ranges 0~10 μm, 10~20 μm, 20~28 μm and 28~34 μm was used to determine the relationship between the depth of the micro-channels and the position of the upper roll. A prototype of the desktop micro rolling machine is shown in Figure 13(a). The pattern depth was measured with an optical microscope (Zyco NewView^{TM} 6300) scanning white-light interferometry (SWLI). A camera detects 3D interferogram data of micro channels. Vertically bipolar scan length is 40 μm, resolution is <0.1 nm, repeatability is <0.3 nm. 2D and 3D surface profile images of the micro-channels with upper roll positions of 34 μm resulted in a channel depth of $\triangle h$=23 μm, as shown in Figure 13(b). The surface texture of the lamina underwent three phases: entrance, rolling and exit. Figure 14(a) shows the upper roll position of y=34 μm and Figure 14(b) shows the rolling forces during the texturing process. The rolling force is defined by $F=F_0+F_1$; i.e.,

$$F=\frac{1}{l_a}\int_0^{l_a}(F_0-F_{0offset})dl+\frac{1}{l_a}\int_0^{l_a}(F_1-F_{1offset})dl \quad (14)$$

where $F_{0offset}$ and $F_{1offset}$ are the offset values of the load cells read at the initial time; F_0 and F_1 are the average values of the load cells read during the rolling process, l_a = 40 mm is the length of the lamina, w_a=20 mm is the width of the lamina.

Subsequent experiments revealed that the upper roll position deviated from y=36 μm, and the PI control system only

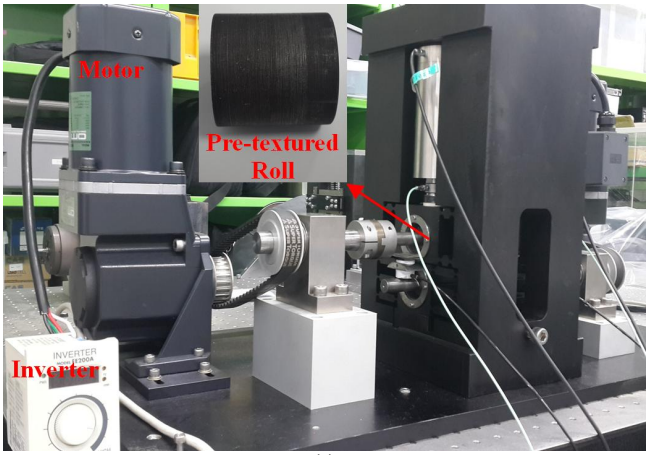

(a)

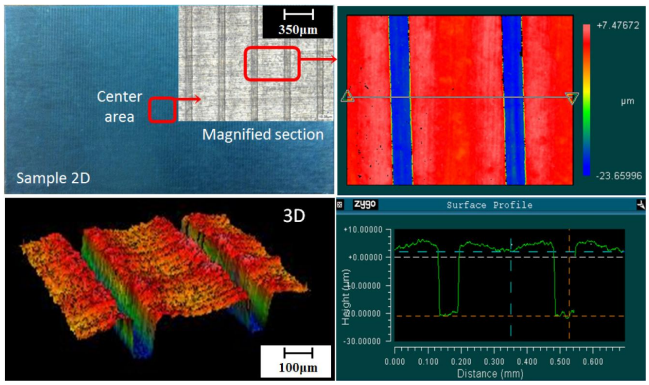

(b)

Fig. 13 (a) A prototype of desktop micro rolling machine & (b) experiment result of the micro-channel depth at position 34 μm of the upper roll

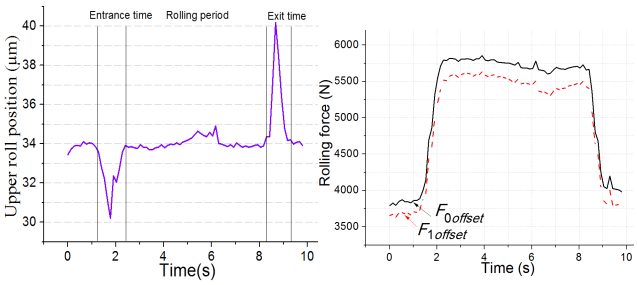

(a) (b)

Fig. 14 (a) the position of the upper roll (b) the force during surface texturing

operated stably with a maximum roll position of y_{max}=35 μm. The results of the channel depth investigations are listed in Table 2.

The linear ranges of the data listed in Table 2 were interpolated to demonstrate the relationship between the depth of the micro-channels and the upper roll position as $\triangle h=a_i \cdot y+b_i$, shown in Figure 15. The depth $\triangle h$ was directly proportional to the upper roll position y, therefore, inversely

Table 2 Experimentally measured depths of the micro-channels

Roll position y (μm)	Channel depth $\triangle h$ (μm)			
	Exp 1	Exp 2	Exp 3	Average
0	8	7	7.5	7.50
10	11	10	9	10.00
20	15.5	14	14.5	14.67
28	18	17.5	17	17.5
34	23	23.5	22.5	23

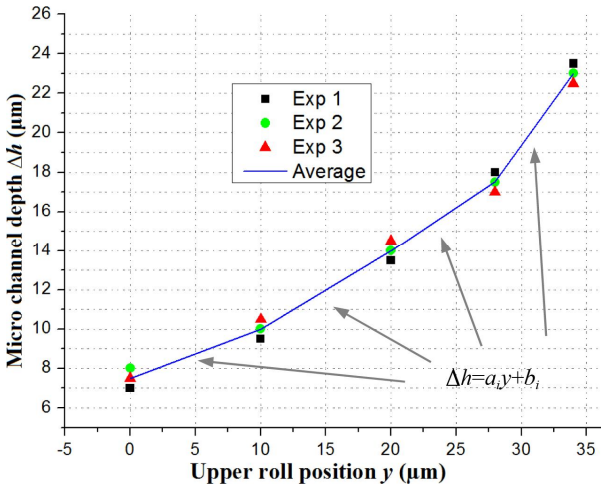

Fig. 15 The relationship between the roll position and the channel depth

proportional to the rolling gap G.

3.4 Position of the Upper Roll to Control Over the Depth of the Micro-channels

From the results obtained in the sections 2.3 and 3.3, the PI control was built for the upper roll position and its relation with the depth was empirically investigated. The position-based deformation control system for the depth of the micro-channels is proposed in Figure 16. If this enables us to establish the feedback signal of channel depth, the control system for the channel depth could be built using the control system for the position of the upper roll. The relationship between the depth of the channels and the position of the upper roller is described by $\triangle h=a_i \cdot y+b_i$, where i=1, 2, 3 or 4, and applied for 4 ranges of y; i.e., 0~10 μm, 10~20 μm, 20~28 μm, 28~34 μm. Using the results listed in Table 2, the values of ai and bi were calculated, and are listed in Table 3.

Experiments were carried out on 1-mm-thick A2021 lamina surfaces using the values of ai and bi listed in Table 3. Fig 17 shows results of the depth input △he and the depth output

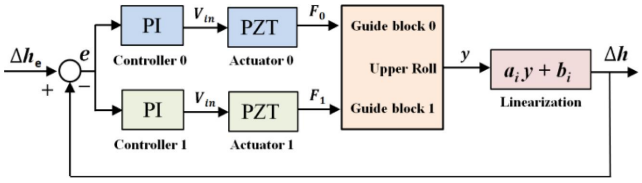

Fig. 16 Scheme of controlling over the micro channel depth in deformation-based surface texturing system

Table 3 Value of the parameters of the linear relationship

i	y (μm)	$\triangle h$ (μm)	a_i	b_i
1	0~10	7.5~10	0.25	7.5
2	10~20	10~14.67	0.467	5.33
3	20~28	14.67~17.5	0.3538	7.595
4	28~34	17.5~23	0.916	-8.1

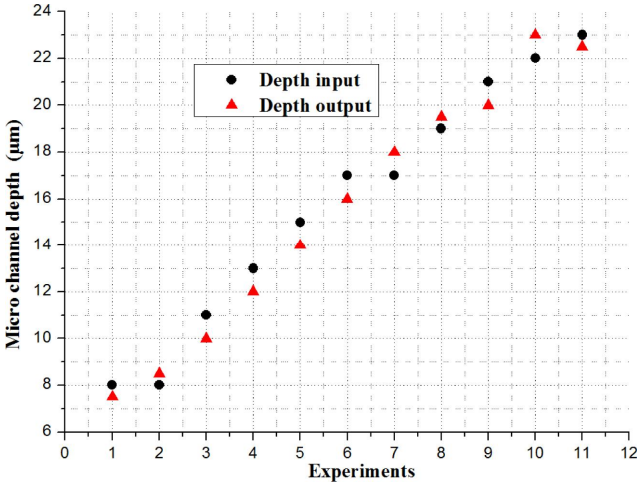

Fig. 17 Experimental results of the micro channel depth

$\triangle h$ in the micro channel deformation control system. Results indicate that the depth output of micro channels $\triangle h$ could be controlled over the range 8~23 μm with a maximum error of 2 μm.

4. Discussions and Conclusions

In this research, the gap between two rollers was initially calibrated to set the parallelism and an initial gap 850 μm along the rolls. PI controllers were proposed to use for positioning the upper roll in the desktop micro-rolling machine (*DμRM*). An empirical method was employed to investigate the relationship between the position of upper roll and the depth of channels which linearly interpolated. Then, a proposed method of controlling over the depth of the micro-channels formed during rolling surface texturing was identified.

Thus, the linear interpolation-based relationship was used to take the feedback signal of depth for developing the control system of the depth through controlling the position of upper roll. The depth of micro-channels was found to control in the range 8 to 23 μm with respect to the position of upper roller from 0 to 34 μm. An error of ±2 μm in the depth along the channels was achieved. This error was attributed to effects of uncertain errors in dimension of the rollers, the roundness of the teeth, parallelism of the rolling gap in dynamic regime and the thickness of the lamina.

The PZT-driven flexure guide block had a low damping ratio, and accurate positioning was achieved using the PI controller. Both the transient and steady-state performance of the closed-loop control system was significantly improved by using the PI controller. The simulation analysis and the experiment results show that the inherent hysteresis in the PZT transducer could be compensated, and the steady state error was eliminated.

For this application, strokes of PZT on upper roll over a range of 0 to 45 μm are used to control the depth of micro-channels. So calibration of the initial rolling gap should be achieved by translating the lower guide block in range of 160 μm. And the wedge unit structure requires an innovation to improve flexibly, accuracy and independence to eliminate the initial tilting error of the rolling gap more precisely.

The deformation-base micro surface rolling system can imprint out various shapes of micro channels by replacing the upper roller. The similar method is applicable to control over the dimension of micro channels in surface texturing process.

Acknowledgement

This work was supported by the Industrial Source Technology Development Program and the International Cooperative R&D Program funded by the Ministry of Trade, Industry and Energy, MOTIE, Korea. The micro-rolling machine design is the result of collaboration with Prof. Kornel Ehmann and Jian Cao in Northwestern University, USA.

References

[1] Choi, H. C., Moin, P., Kim, J., 1993, Direct Numerial Simulation of Turbulent Flow Over Riblets, J. Fluid Mech., 255 503-539.

[2] Ashwin, R., Wasim, A., Surya, P. M., Andrew, H. C., Andreas, A. P., William, P. K., 2013, Friction Characteristics of Micro-textured Surfaces under Mixed and Hydrodynamic Lubrication, Tribology Int., 57 170-176.

[3] Rashwan, O. H., Stoilov, V., Alpas, A. T., Guerrero, A. R., 2012, Effect of Surface Patterning on the Adhesive Friction, ASME Int. Mech. Eng. Cong. & Exp., 3 2117-2124.

[4] Sahlin, F., Glavatskih, S. B., Almqvist, T., Larsson, R., 2005, Two-dimensional CFD-Analysis of Micro-patterned Surfaces in Hydrodynamic Lubrication, Trans. of the ASME, 127:1 96-102.

[5] Aviram, R., Izhak, E., Yuri, K., 2001, Friction-reducing Surface-texturing in Reciprocating Automotive Components, Tribology trans., 44:3 359-366.

[6] Shinkarenko, A., Kligerman, Y., Etsion, I., 2009, The Effect of Surface Texturing in Soft Elasto-hydrodynamic Lubrication, Tribology Int., 42:2 284-292.

[7] Christos, I. P., Pantelis, G. N., Lambros, K., 2011, Evolutionary Optimization of Micro-Thrust Bearings with Periodic Partial Trapezoidal Surface Texturing, J. of Eng. for Gas Turb. and Pow., 133:1 1-9.

[8] Etsion, I., 2005, State of the Art in Laser Surface Texturing, Journal of Tribology, 127:1 248-253.

[9] Allen, D. M., 2004, Photochemical Machining: From 'Manufacturing's Best Kept Secret' to a $6 Billion Per Annum, Rapid Manufacturing Process, CIRP Annals-Manuf. Tech., 53:2 559–572.

[10] Hirt, G., Thome, M., 2007, Large are Rolling of Functional Metallic Micro Structures, Prod. Eng. Res. and Dev., 1 351-356.

[11] Zhou, R., Cao, J., Ehmann, K., Xu, J., 2011, An Investigation on Deformation-based Micro Texturing System, J. Manuf. Sci E-T ASME, 133 1-6.

[12] Macki, J.W., Nistri, P., and Zecca, P., 1993, Mathematical Models for Hysteresis, SIAM Review, 35 1 94–123.

[13] Smith, S. T., 2000, Flexures: Elements of Elastic Mechanisms, Gordon and Breach Science Publishers, Amsterdam, 177-192.

[14] Howell, L. L., 2001, Compliant Mechanism, Wiley-IEEE, 38-53.

[15] Ryu, S. O., Kim, H. Y., Ahn, J. H., 2014, Characteristics of a PZT-driven Micro Depth Adjustment Device for Cutting Coated Film, Journal of the KSMTE, 23:6 630-635.

[16] Choi, K. B., Lee, J. J., Kim, G. H., Lim, H. J., 2011, A Piezo-driven Ultra-precision Stage for Alignment Process of a Contact-type Lithography, Journal of the Korean Society of Manufacturing Technology Engineers, 20:6 756-760.

[17] Paros, J., and Weisbord, L., 1965, How to Design Flexure Hinges,

Machine Design, 37:27 151-156.

[18] Li, Y., Xiao, X. L., Wu, Z. G., 2014, Design, Modeling, Control and Experiment for a 2-DOF compliant Micro-motion Stage, Int. J. of Pre. Eng. and Manuf., 15:4 735-744.

[19] Liaw, H. C., Shirinzadeh, B., 2008, Enhanced Adaptive Motion Tracking Control of Piezo-actuated Flexurebased Four-bar Mechanisms for Micro/Nano Manipulation, Sensors and Actuators A: Physical, 147:1 254-262.

[20] Wang, H., Zhang, X., 2008, Input Coupling Analysis and Optimal Design of a 3-DOF Compliant Micro-positioning Stage, Mechanism and Machine Theory, 43:4 400-410.

[21] Lin, C. J., Lin, P. T., 2012, Tracking Control of a Biaxial Piezo-actuated Positioning Stage using Generalized Duhem Model, Computers and Mathematics with Applications, 64:5 766-787.

[22] Tan, K. K., Lee, T. H., Zhou, H. X., 2001, Micro-positioning of Linear-piezoelectric Motors based on a Learning Nonlinear PID Controller, IEEE/ASME Transactions on Mechatronics, 6:4 428-436.